Investigation of the Shape and Size of Myosin Subfragment 1 Using Small-Angle X-Ray Scattering†

K. M. Kretzschmar,‡ R. A. Mendelson, and M. F. Morales*,§

ABSTRACT: Measurement of x-ray scattering at very small angles by solutions of myosin subfragment 1 (S1) yields a radius of gyration of 3.24 nm (mean) ± 0.03 nm (standard error for $N = 9$). If S1 is assumed to be ellipsoid of revolution, of uniform electron density, with a molecular weight of 1.15×10^5 and a partial specific volume of 0.73 $cm^3\ g^{-1}$, then the axial ratio of the ellipsoid is 2.89 ± 0.06 (prolate) or 0.26 ± 0.01 (oblate), and the major axis is 13.0 ± 0.2 nm (prolate) or 10.1 ± 0.1 nm (oblate). Measurements at larger angles allow models of S1 morphology to be tested; theoretical scattering curves for various ellipsoids of revolution were calculated. The observed scattering can be approximated by the scattering from ellipsoids with axial ratio 2.0 to 3.0 (prolate), or 0.25 to 0.4 (oblate). Models that fit the data over the range of scattering angles from 0 to 30 mrad are: prolate ellipsoid with axial ratio 2.3, major axis 12 nm; and oblate ellipsoid with axial ratio 0.4 and major axis 10 nm. Thus analyses of two parts of the scattering curve, by different methods, indicate that S1 is far from spherical, and that its morphology may be approximated by ellipsoids of the aforesaid dimensions.

The tension that is generated during the contraction of skeletal muscle is thought to be a result of the interaction of actin and myosin filaments (Gordon et al., 1966). More specifically, this interaction is thought to occur between actin filaments and projections from the myosin filament known as cross-bridges (Huxley, 1963). The part of the myosin molecule that binds to actin and exhibits ATPase activity is known as subfragment 1 (S1)[1] (Müeller & Perry, 1962). S1 is a substantial part of the cross-bridge and is a structure of central importance to the understanding of muscular contraction. Unfortunately, the shape and size of S1 are uncertain at present: Lowey et al. (1969), using electron micrographs, estimated that S1 is a sphere of diameter 7 nm. Moore et al. (1970), using image-reconstructed micrographs of F-actin decorated with S1, believe that S1 has the shape of a bent rod. Mendelson et al. (1973), using the rotational diffusion coefficient, take S1 to be prolate ellipsoid, with major axis 16 nm long. Their conclusion that S1 is elongate was confirmed by Thomas et al. (1975), using saturation transfer electron paramagnetic resonance. Lymn & Cohen (1975) favor a relatively long cross-bridge; Haselgrove et al. (1976) do not. A clearer understanding of S1 morphology would allow existing results to be interpreted more precisely: For example, fluorescence data from muscle (Tregear & Mendelson, 1975; Borejdo & Putnam, 1977) and from muscle proteins (Mendelson et al., 1973) could reveal the orientation of the fluorophore relative to the S1 molecule, and hence cross-bridge attitude, and movement could then be measured. X-ray diffraction data from living muscle yields information concerning the structure of the thick filament. However, without a knowledge of the shape of the cross-bridge, the data cannot be interpreted with certainty, and a number of different structures for the thick filament have been proposed, e.g., Huxley & Brown (1967) and Squire (1972).

This paper describes an investigation of the morphology of S1 using the scattering of x-rays at small angles by S1 solutions; a preliminary description of this work has been published (Kretzschmar et al., 1977). The theory of such scattering has been developed extensively (Guinier & Fournet, 1955; Beeman et al., 1957; Kratky & Pilz, 1972).

Experimental Procedures

Preparation of Subfragment 1. S1 was prepared from myosin by digestion with insoluble papain at room temperature (composition of digestion mixture: 0.04 mol/L KCl, 2 mmol/L dithiothreitol, 5 mmol/L EDTA, 12 mg/mL myosin, typically 25 μg/mL papain, pH 7). Digestion was arrested after 20 min by centrifugation followed by treatment with 100 mol/L *N*-α-*p*-tosyl-L-lysine chloromethyl ketone HCl. The supernatant was filtered through a Sephadex G200 column in 0.15 mol/L KCl, 10 mmol/L *N*-tris(hydroxymethyl)methylamino-2-aminoethanesulfonic acid (Tes), pH 7. Preparations were characterized by: 10% sodium dodecyl sulfate–polyacrylamide gel electrophoresis, analytical ultracentrifugation, and ATPase measurements (reaction mixture: 0.55 mol/L KCl, 45 mmol/L tris(hydroxymethyl)aminomethane (Tris), 9 mmol/L $CaCl_2$, 0.9 mmol/L Na_2H_2 ATP, pH 8. 25 °C).

Measurement of the Intensities of X-Rays Scattered at Small Angles. An apparatus (Figure 1) was designed for use at the Stanford Synchrotron Radiation Project. The incident beam consisted of a continuous spectrum of x-ray photons, with energies of 3 to 30 keV. This beam was diffracted at a Bragg angle of 45° by a silicon crystal, thus eliminating all but a series of discrete bands of energy (Pianetta & Lindau, 1978). Only the band of lowest energy (8.37 keV, bandwidth 0.1 keV), the

† From the Cardiovascular Research Institute, University of California, San Francisco, California 94143. *Received October 31, 1977.* Supported by U.S. Public Health Service, Program Project Grants HL-16683 and HL-06285, National Science Foundation Grants GB 24922X, PCM 75-22698, and PCM 76-11491, and partially by National Science Foundation Grant DMR 73-07692, in cooperation with SLAC and ERDA.

‡ K. M. Kretzschmar was initially a fellow of the Science Research Council (U.K.) and is now a Visiting Scientist of the American Heart Association.

§ M. F. Morales is a Career Investigator of the American Heart Association.

[1] Abbreviations and symbols used: SE, standard error; SD, standard deviation; S1, subfragment 1 of myosin; fwhm, full width at half maximum; $h = (4\pi/\lambda)\sin(\theta/2)$; λ, the x-ray wavelength; θ, the angle between scattered and unscattered beams; $i(h)$, the intensity of scattering, normalized to 1 at $h = 0$; γ, the axial ratio (a/b) of an ellipsoid with semiaxes a, b (prolate ellipsoid $\gamma > 1$, oblate $\gamma < 1$); R, the particle radius of gyration; dV, a volume element of electron density ρ, a distance r from the center of electron mass of the particle; m, the slope of the Guinier plot; DTNB, 5,5′-dithiobis(2-nitrobenzoic acid).

0006-2960/78/0417-2314$01.00/0

result of a 333 reflection, was used for scattering data. Consequently this band was isolated from bands of higher energy (11.18 keV, 13.95 keV, and larger). Electronic discrimination alone sufficed to eliminate bands with energies of 13.95 keV and larger and was almost adequate to eliminate the band at 11.18 keV. However, to ensure that the latter was excluded, a copper foil (25 μm thick) was used as a filter, since copper absorbs radiation preferentially at this energy. The energy of the 8.37-keV band was calculated from the lattice dimensions of the silicon crystal and was confirmed experimentally using a Si(Li) solid state detector. Synchrotron radiation is intrinsically collimated; the divergence of the beam, in the direction in which scattering measurements were made, was 0.2 mrad, fwhm. Consequently no further collimation was required. The beam was shaped by a single defining slit to provide the appropriate angular resolution at the detector. The use of a guard slit, thin sample cell windows, appropriate slit edge design, and a helium atmosphere enabled the parasitic scattering to be kept low, so that it only had a small adverse effect on the statistical accuracy of measurement. A position sensitive detector (PSD 100, Tennelec; detector gas 3% CO_2, 97% Ar at 0.6 MPa) was used to reduce exposure times. The detector measured both the position at which a photon was detected (spatial resolution: 200 μm fwhm) and the energy of that photon (energy resolution: 20% of photon energy, fwhm). Signals from the position sensitive detector were processed by standard electronics (PSD 100 system, Tennelec), except that an automatic gain control amplifier (NA22, Harshaw) was used to stabilize the energy spectrum before discrimination. Data were collected using a multichannel analyzer. Count rates were 1000/s or less, and, under these conditions, electronic pileup proved insignificant. The sample cell was maintained at 1 °C to avoid denaturation of S1.

Data Processing. Calibrations relating photon position to channel of the multichannel analyzer were performed routinely by placing a slotted mask over the detector. The variation of efficiency (the probability of detection of a photon) with photon position was measured using the strong isotropic fluorescence of iron when it was illuminated by radiation of about 8 keV. The data were corrected for small changes in efficiency where required. The primary beam was plane polarized, but calculations show this had a negligible effect on measurements at the small angles of scattering reported here.

In order to measure the scattering due to S1 it was necessary to collect data on both a solution of S1 and on solvent alone. In general these two measurements were not the result of identical exposures to x-rays. Consequently the intensity of scattering by solvent was corrected by a factor such that the two sets of data became coincident at large angles of scattering (>85 mrad), where no differences were anticipated. Subtraction of this corrected solvent scattering from the scattering by S1 solution at each angle of scattering yielded the scattering due to S1 alone.

Models for the Shape of S1. Scattering curves for various ellipsoids of revolution were calculated according to the equation of Porod (1948):

$$i(h) = \sum_{n=0}^{\infty}\left[(-1)^n 72\frac{(2n+2)(2n+5)}{(2n+6)!}2^{2n}\left(\frac{5}{2+\gamma^2}\right)^n \sum_{r=0}^{n}\frac{n!}{r!(n-r)!}\frac{(\gamma^2-1)^r}{2r+1}\right](hR)^{2n} \quad (1)$$

where $h = (4\pi/\lambda)\sin(\theta/2)$; λ is the x-ray wavelength; θ is the angle of scattering (angle between scattered and unscattered beams); $i(h)$ is the intensity of scattering, normalized to 1 at $h = 0$; γ is the axial ratio (a/b) of the ellipsoid with semiaxes

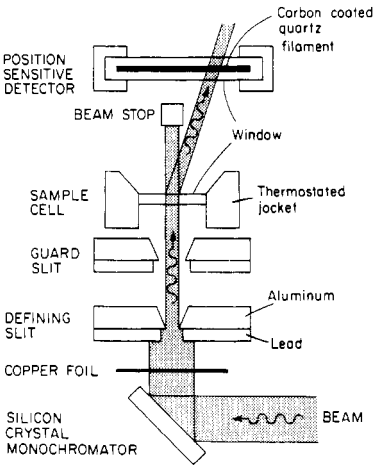

FIGURE 1: Apparatus for measurement of small-angle x-ray scattering. For clarity the diagram is not to scale. Typical dimensions are: defining slit to sample cell, 450 mm; sample cell to detector, 450 mm; guard slit to sample cell, 20 mm; x-ray path length in sample cell, 1 mm; defining slit typically 10 mm × 1.5 mm; active area of position sensitive detector, 60 × 4 mm; source to detector, 14 m.

a, b, and b (prolate ellipsoid $\gamma > 1$, oblate $\gamma < 1$); R is the radius of gyration.

In general:

$$R^2 = \frac{\int_v r^2\rho dV}{\int_v \rho dV} \quad (2)$$

where dV is a volume element of the particle, of electron density ρ, a distance r from the center of electron mass of the particle. The integral is taken over the volume (V) of the particle. Derivation of eq 1 assumes ρ to be constant. A scattering curve obtained from eq 1 is that resulting from a beam of infinitely small cross-section, detected with prefect spatial resolution. Of course, in practice beam dimension (given in Figure 1) and detector resolution (given above) were finite. Therefore the calculated curves were convoluted with these beam and detector parameters before comparison with experimental curves. This method is preferable to the more conventional technique of deconvoluting the experimental curve; the calculation is substantially simpler and does not require boundary assumptions, and the generation of spurious oscillations in the scatter diagram is not possible. For calculating smearing the beam cross-section at the sample and the detector were considered as arrays of rectangular elements. The rectangles were chosen small enough so that no significant smearing results from the scattering of one element of beam into one element of detector. The scattering for each pair of beam and detector elements was calculated, and then a sum for all such pairs of elements was formed. The detector area was defined by the detector resolution.

Results

Validation of Methods. The elution curve of material filtered through the Sephadex column exhibited a sharp, well-separated S1 peak. The ATPase activity was constant across the peak, suggesting that S1 was pure. The Ca^{2+}-ATPase activity was 15.1 ± 1.2 μmol g^{-1} s^{-1} (mean and SE, $N = 9$, six preparations of S1), a value compatible with that of myosin under these conditions. Sodium dodecyl sulfate-polyacrylamide gel electrophoretograms exhibited the known properties of S1 (Weeds & Lowey, 1971). All three light chains were

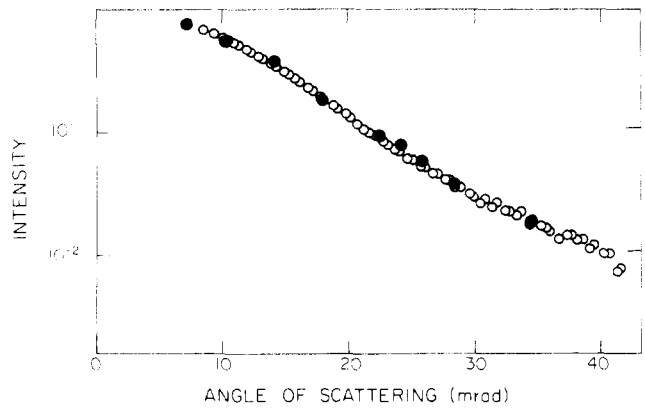

FIGURE 2: X-ray scattering by a 5% solution of bovine serum albumin. The intensity of scattering is normalized to 1 at zero angle of scattering. (●) From Anderegg et al. (1955, Figure 6) and corrected for slit dimensions. (○) Present results, using slit dimensions such that no corrections were required.

present, with appropriate molecular weights. The DTNB light chain was at very low concentration as expected, since papain proteolysis occurred in the absence of Mg ion. The A1 light chain has a slightly reduced molecular weight. A small fraction of the heavy chain was degraded to produce a second heavy chain band of slightly lower molecular weight. One preparation of S1 was studied in the ultracentrifuge. The sedimentaion coefficient (corrected for temperature and viscosity of solvent) was almost identical with that reported by Lowey et al. (1969). A small amount of high molecular weight contamination was detectable, but was difficult to quantify; it represented less than 10% by weight of the total protein.

Methods for measurement of x-ray scattering were validated using solutions of bovine serum albumin (Sigma, product no. A4503). Figure 2 shows a comparison of our results with those employing entirely different instrumentation (Anderegg et al., 1955). There is excellent agreement between the two sets of measurements, suggesting that data obtained by our methods are valid.

Two tests were made for radiation damage of S1. Firstly, samples of S1 were subjected to large doses of radiation, by irradiating the whole area of a sample cell (75 mm^2) for about 1 h. The ATPase activities of samples tested after the exposure were indistinguishable from those of nonirradiated samples taken from the stock solution. Secondly, the scattering measured during the first 30 min exposure was compared with the scattering measured in a 30-min period following 140 min of irradiation. The two curves were indistinguishable. Thus neither test indicated any radiation damage. All samples used to provide morphological information were irradiated for 1 h or less, using a beam cross-sectional area of about 10 mm^2.

Scattering at Angles of 5 to 10 mrad. The shape of the scattering curve due to particles in a monodisperse solution is independent of particle shape at sufficiently small angles of scattering (Guinier & Fournet, 1955, pp 24–28). In the limit of small angles and low concentration the intensity of scattering is given by:

$$i(h) = \exp(-h^2R^2/3) \qquad (3)$$

In the case of a molecule of the size of S1, it is reasonable to expect that this (Guinier) approximation might apply in the range of scattering angles from zero to about 12 mrad. However, the range over which the approximation holds depends not only on the size, but also on the shape of S1; therefore, the validity of this expectation must be tested. Figure 3 shows a plot of $\log[i(h)]$ against θ^2 for one set of data. Such Guinier

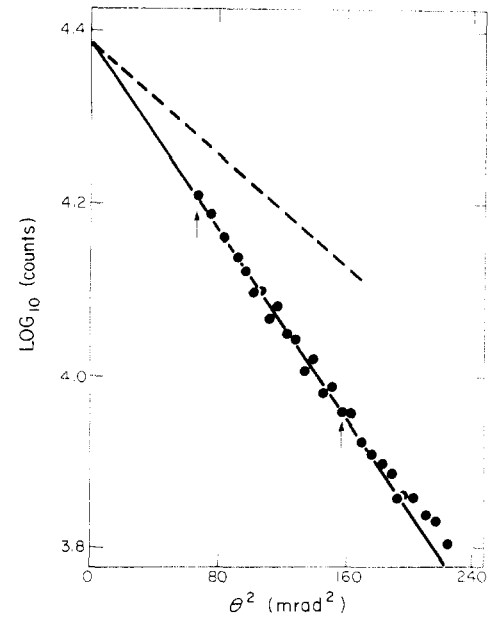

FIGURE 3: Guinier plot for one sample of S1. (●) Experimental points. The standard deviations due to counting errors are smaller than or approximately equal to the radius of the symbol used to depict the data. The solid line is the linear regression taken between the limits indicated by the arrows. The slope of this line corresponds to a radius of gyration of 3.22 nm. The broken line indicates the slope of the scattering curve calculated assuming S1 to be spherical, as described more fully in the discussion.

plots are linear at small angles for monodisperse solutions. It can be seen from eq 3 that the radius of gyration of S1 (eq 2) is related to the slope (m) of the region of the plot over which the Guinier approximation holds:

$$R = \frac{\lambda}{\pi}\sqrt{-m}\left(\frac{3 \ln 10}{4}\right)^{1/2} \qquad (4)$$

Using this equation the radius of gyration of S1 from five preparations was found to be 3.24 nm (mean) ± 0.03 nm (SE for $N = 9$). The measurements confirm previous results, obtained using a (movable, position insensitive) NaI(Tl) detector (Kretzschmar et al., 1976).

The Guinier plots were found to be linear for values of the abscissa up to at least 160 $mrad^2$. Thus this value was used as the upper limit in the determination of the radius of gyration. A lower limit of 60 $mrad^2$ was set by the size of the beam stop in many instances. In some experiments the scattering at 60 $mrad^2$ was affected by small amounts of aggregates in the sample. In the worst case this deviation from linearity at very small angles indicated that the aggregates amounted to 5% by weight of the protein present. In the instances where contamination was present the lower limit was chosen at a value greater than 60 $mrad^2$, so that aggregates had negligible effect on the linearity of the Guinier plots. The scattering at all angles greater than this lower limit was independent of the degree of contamination, as was expected from theoretical estimates of the effects of aggregates.

No dependence of the measured radius of gyration upon the concentration of S1 was found: the slope of the regression of R vs. concentration was −0.0042 nm mg^{-1} mL (SD = 0.0057, $N = 9$, concentration range 1.8–18.0 mg/mL). This is to be expected since we were able to use low protein concentrations at which interparticle interactions are very small (Lowey et al., 1969).

Scattering at Angles Up to 30 mrad. More detailed information about the shape of S1 is obtained at the larger angles of scattering at which the Guinier approximation no longer

holds. At these angles, the scattering due to S1 is much less intense than at smaller angles (intensity of scattering at 30 mrad is 2% of that at zero angle). It is also less intense than the scattering due to solvent (at 30 mrad it is 20% of that due to solvent). Therefore, in order to make accurate measurements, the number of photons detected must be large. Accordingly, for these larger angle measurements, the slit dimensions were adjusted so that the count rate was high (ca. 500/s), but electronic pileup remained negligible and angular resolution was adequate. The intrinsic collimation of the x-ray beam provides greater available intensity; a given angular resolution results from a slit area about tenfold greater than that required if an extended divergent source were used. Adequate statistical accuracy was obtained using exposures of a few hours. In contrast, similar measurements, using an x-ray tube and a position insensitive detector, would require exposures lasting many days. Figure 4 shows the raw data obtained for one preparation of S1. Measurements using three preparations showed no significant differences between preparations, and results were independent of concentration in the range investigated (2.5 to 8 mg/mL).

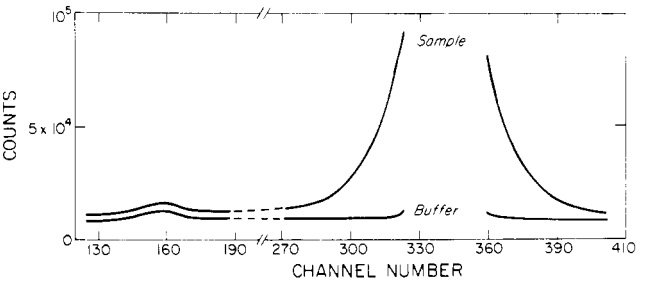

FIGURE 4: Raw data obtained from one preparation of S1. The intensities of scattering (counts) detected at each position within the detector were stored in a multichannel analyzer. The upper and lower curves were obtained using a solution of S1 (7.9 mg/mL) and solvent, respectively. The scattering due to S1 alone is obtained by subtraction, after correction for differences in exposure as described in the text. Channels 323 to 360 correspond to the position of the beam stop. The peak at channel 160 is caused by the windows of the sample cell.

Discussion

Sources of Error. Measurements on a well-characterized substance, bovine serum albumin, validate our methods of measurement and data processing (see Figure 2). The first stage in our data processing, viz., the correction for differences in the exposures of sample and solvent, is unconventional, so further testing of this procedure is desirable. This is possible since the raw data (Figure 4) contain a diffuse Bragg reflection at a scattering angle ca. 90 mrad, produced by the windows of the sample cell. If there were significant scattering by S1 in the region of this Bragg peak, then the curves for sample and solvent could not be made to match in this region by multiplying all the intensities in one set of data by a single correction factor. In fact such a correction factor does bring the two curves into congruence within statistical error. Therefore S1 produces no significant scattering in the region of the Bragg peak, and it is legitimate to take the scattering due to sample and solvent to be coincident over this region. The advantage of curve-matching over using a separate system to monitor beam intensity, is that a number of possible errors is avoided. For example, errors are not caused by changes in efficiency of detection, changes in the spectrum of the primary beam, of electronic changes such as a change in the dead time of the multichannel analyzer or drift of the energy discrimination system.

The Radius of Gyration of S1. The volume of S1 may be calculated assuming a molecular weight of 1.15×10^5 (Lowey et al., 1969) and a partial specific volume of 0.73 $cm^3\ g^{-1}$, that is characteristic of globular proteins (Sakura & Reithel, 1972; see below). Figure 3 shows a plot of the scattering by S1 in the Guinier region and the scattering calculated for a spherical molecule with a molecular volume equal to that of S1. Clearly there is a large discrepancy between the two plots, and thus S1 is not even approximately spherical.

The measured radius of gyration of S1 ($R = 3.24 \pm 0.03$ nm, mean $\pm$ SE, $N = 9$) specifies models characterized by a single parameter. For example, S1 may be assumed to be an ellipsoid of revolution of uniform electron density. Then R constrains the ellipsoid to have an axial ratio of 0.26 ± 0.01 (for an oblate ellipsoid) or 2.89 ± 0.06 (for a prolate ellipsoid), and a major axis of 10.1 ± 0.1 nm (oblate) or 13.0 ± 0.2 nm (prolate). The value of the partial specific volume used in the foregoing calculation (0.73 $cm^3\ g^{-1}$) happens also to be that of myosin polypeptide chains that do not enclose interstices. However, once R is fixed the percent change in either axial ratio or major axis is equal to, or less than, the percent change in partial specific volume. Since the range of the latter has a breadth of ca. 3%, the choice of this parameter has but a small effect on the dimensions that we are reporting.

The Adequacy of Ellipsoids of Revolution as Models for the Shape of S1. The models considered above were restricted to a particular molecular volume and were tested using the scattering at very small angles only. Measurements at larger angles of scattering allow less restricted models of S1 morphology to be tested. Scattering curves for prolate and oblate ellipsoids of revolution are shown in Figure 5. In calculating these curves the value of R was kept constant at 3.2 nm and it was assumed that the ellipsoids were of uniform electron density. However, no assumptions as to molecular volume, molecular weight, or partial specific volume were necessary. Figure 5 also shows experimental data obtained for S1 at these large angles. Intensities and angles of scattering are normalized (as described in the figure legend) so that curves become independent of molecular size or density, and express only molecular shape. The experimental curve is not a member of either family of theoretical curves, i.e., the data cannot be fitted within random error. However, close fits are obtained for axial ratios of 2.3 (prolate) and 0.4 (oblate). It is interesting that, when the molecular volume is determined by the model, the value obtained is somewhat larger than that calculated for a molecular weight of 1.15×10^5 and a partial specific volume of 0.73 $cm^3\ g^{-1}$. This may indicate that S1 possesses internal water of hydration (29% and 39% for the prolate and oblate models, respectively), or more likely, that ellipsoids are inadequate models in this respect.

The Accuracy of the Guinier Approximation. The observation that the Guinier plots are linear, over the range of scattering angles used to calculate R, suggests that the Guinier approximation (eq 3) is accurate over this range. However, there is another test of the accuracy of this approximation. For a given model, the error in R may be calculated. For the models discussed above the errors are small, e.g., for a prolate ellipsoid with an axial ratio of 2.3, R is underestimated by about 3.5%; for an oblate ellipsoid with an axial ratio of 0.26, R is underestimated by about 1%.

In summary, the results show that S1 is not precisely ellipsoidal, but the observed scattering can be *approximated* by the scattering from ellipsoids of the dimensions given above. Analyses of two parts of the scattering curve, by different methods, indicate that S1 is far from spherical, and that its shape may be approximated by ellipsoids of axial ratio ca. 2.5,

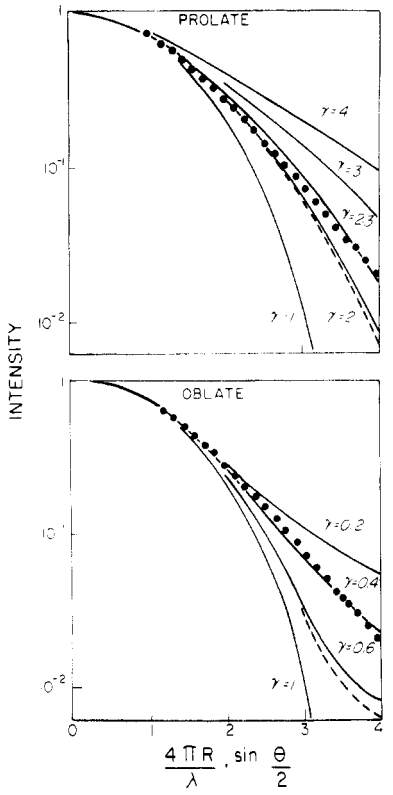

FIGURE 5: Ellipsoids of revolution of constant radius of gyration as models for the shape of S1. The solid lines show the scattering calculated for prolate and oblate ellipsoids of revolution, axial ratio γ, convoluted with slit and detector parameters. The broken lines show unconvoluted curves. (●) Scattering due to S1. All intensities are normalized to 1 at zero angle. Counting errors are negligible and cannot be shown since they are smaller than the symbols used to depict the data. R is the radius of gyration of S1 (3.2 nm). λ is the wavelength of x-rays (0.148 nm). θ is the angle of scattering.

major axis ca. 12.5 nm (prolate) or axial ratio ca. 1/3, major axis ca. 10 nm (oblate).

The restrictions that the present results place on the dimensions of S1 bear on the interpretation of existing results. Analyses of x-ray diffraction data that have assumed the cross-bridge to be small and spherical (Huxley, 1969; Haselgrove et al., 1976) require revision, whereas those that used an elongated model for the cross-bridge (Squire, 1972; Miller & Tregear, 1972) are compatible with the present results. Fluorescence depolarization measurements (Mendelson et al., 1973) were analyzed by assuming S1 to be a prolate ellipsoid and gave a major axis of at least 16 nm. This estimate was for a hydrated particle; an external layer of immobilized water would not affect x-ray scattering measurements, so the latter technique might well lead to a lower estimate. Furthermore the method of preparation for the fluorescence work may well have yielded a higher molecular weight S1, containing a higher content of DTNB light chain than the S1 used in the present investigation. Consequently a slightly larger value for major axis length might be expected to result from the fluorescence measurements. Since the present results show that S1 is not precisely ellipsoidal, there is no reason to expect that the equivalent ellipsoid required to describe hydrodynamic properties should be precisely the same as the equivalent ellipsoid that yields the radius of gyration measured by x-ray scattering techniques. Therefore measurements of S1 using either fluorescence or x-ray methods agree as well as might be expected.

Acknowledgments

We wish to thank Margaret Davenport for her tireless assistance with the biochemical preparations, Professor J. W. Anderegg for advice concerning x-ray apparatus design, the staff at SSRP, particularly Professors S. Doniach, A. Golde, R. Filippi, E. Moss, Dr. P. Pianetta, and B. Salsburg and Dr. H. Winick for their invaluable help, and Professor O. Kratky for helpful comments during the preparation of this manuscript.

References

Anderegg, J. W., Beeman, W. W., Shulman, S., & Kaesberg, P. (1955) *J. Am. Chem. Soc. 77,* 2927.

Beeman, W. W., Kaesberg, P., Anderegg, J. W., & Webb, M. B. (1957) *Handb. Physiol. 32,* 321.

Borejdo, J., & Putnam, S. (1977) *Biochim. Biophys. Acta 459,* 578.

Gordon, A. N., Huxley, A. F., & Julian, F. J. (1966) *J. Physiol. 184,* 170.

Guinier, A., & Fournet, G. (1955) *Small Angle Scattering of X-Rays,* Wiley, New York, N.Y.

Haselgrove, J. D., Stewart, M., & Huxley, H. E. (1976) *Nature (London) 261,* 606.

Huxley, H. E. (1963) *J. Mol. Biol. 7,* 281.

Huxley, H. E. (1969) *Science 164,* 1356.

Huxley, H. E., & Brown, W. (1967) *J. Mol. Biol. 30,* 383.

Kratky, O., & Pilz, I. (1972) *Q. Rev. Biophys. 5,* 481.

Kretzschmar, K. M., Mendelson, R. A., & Morales, M. F. (1976) *Biophys. J. 16,* 126a.

Kretzschmar, K. M., Mendelson, R. A., & Morales, M. F. (1977) *Biophys. J. 17,* 36a.

Lowey, S., Slayter, H. S., Weeds, A. G., & Baker, H. (1969) *J. Mol. Biol. 42,* 1.

Lymn, R. W., & Cohen, G. H. (1975) *Nature (London) 258,* 770.

Mendelson, R. A., Morales, M. F., & Botts, J. (1973) *Biochemistry 12,* 2250.

Miller, A., & Tregear, R. T. (1972) *J. Mol. Biol. 70,* 85.

Moore, P. B., Huxley, H. E., & DeRosier, D. J. (1970) *J. Mol. Biol. 50,* 279.

Müeller, H., & Perry, S. V. (1962) *Biochem. J. 85,* 431.

Pianetta, P., & Lindau, I. (1978) *J. Electron Spectros.* (in press).

Porod, G. (1948) *Acta Phys. Austriaca 2,* 255.

Sakura, J. O., & Reithel, F. J. (1972) *Methods Enzymol. 26,* 107.

Squire, J. M. (1972) *J. Mol. Biol. 72,* 125.

Thomas, D. D., Seidel, J. C., Gergely, J., & Hyde, J. S. (1975) *J. Supramol. Struct. 5,* 376.

Tregear, R. T., & Mendelson, R. A. (1975) *Biophys. J. 15,* 455.

Weeds, A. G., & Lowey, S. (1971) *J. Mol. Biol. 61,* 701.